Geomorphology 458 (2024) 109227

Contents lists available at ScienceDirect

Geomorphology

journal homepage: www.journals.elsevier.com/geomorphology

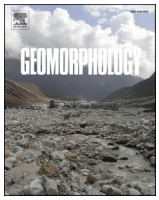

CoMMa: A GIS geomorphometry toolbox to map and measure confined landforms

Riccardo Arosio [a,b,*], Joana Gafeira [c], Laurence H. De Clippele [d], Andrew J. Wheeler [a,b,e], Veerle A.I. Huvenne [f], Fabio Sacchetti [g], Luis A. Conti [h], Aaron Lim [a,b,i]

[a] School of Biological, Earth and Environmental Sciences, University College Cork, Ireland
[b] Environmental Research Institute, University College Cork, Ireland
[c] British Geological Survey, The Lyell Centre, Edinburgh, United Kingdom
[d] School of Biodiversity, One Health and Veterinary Medicine, University of Glasgow, United Kingdom
[e] SFI Centre for Research in Applied Geosciences, University College Cork, Ireland
[f] National Oceanography Centre, Southampton, United Kingdom
[g] Marine institute, Oranmore, Galway, Ireland
[h] Universidade de São Paulo, São Paulo, Brazil
[i] Department of Geography, University College Cork, Ireland

ARTICLE INFO

Keywords:
Geomorphometry
Semi-automation
Geomorphology mapping
Digital elevation model
GIS

ABSTRACT

The Confined Morphologies Mapping (CoMMa) Toolbox, a novel ArcGIS Pro python toolbox expressly created for semi-automated seabed morphological mapping, is presented here. The toolbox includes a selection of tools for the pre-processing, delineation and description of confined features on a digital elevation model (DEM) that are either negative or positive. The CoMMa Toolbox addresses the need for a flexible and multi-faceted solution applicable to different mapping problems, also encapsulating and re-interpreting existing methodologies. This study also evaluates, qualitatively and quantitatively, the performance of CoMMa delineations performed on a synthetic bathymetry DEM with 150 coral mounds of known characteristics against manual digitisations completed by five expert geomorphologists. The results show that the best CoMMa delineation falls within the range of competence demonstrated by the expert manual mappers. Edge evaluation metrics and attribute error scores are comparable or often superior to four of the five human delineations, although the Toolbox never reaches the performance of the best expert. Nevertheless, the semi-automated techniques can be of assistance to any user, providing rapid, visually unbiased and consistent delineations, thus saving time: they can then be optimised manually where desirable. Moreover, while the toolbox was created for marine geomorphometry, it can be applied to any DEM, either marine, terrestrial or extra-terrestrial.

The CoMMa Toolbox is available in a public GitHub repository with a thorough user guide.

1. Introduction

Marine geoscientists and seabed habitat mappers are heavily dependent on digital elevation models (DEMs) to delineate and describe seabed landforms. An accurate, quantitative geomorphometric knowledge of seabed landscapes is critical to recognize patterns within landform populations (e.g. pockmarks, drumlins or coral mounds), which in turn helps understanding the landform-seabed relationships, formation mechanisms and potential environmental drivers (De Clippele et al., 2017; Gafeira et al., 2012). Moreover, it provides robust baseline information that assists in a suite of applications for offshore development or habitat mapping (Arosio et al., 2021; Goes et al., 2019; Linklater et al., 2019).

The ever-growing amount of high-resolution bathymetry data produced by modern geophysical surveys requires the application of consistent and time-saving analytical methods, that can process vast numbers of landforms producing replicable results for inter-mapping comparisons. A solution has been found in the development of GIS-based semi-automated tools or techniques, that can quickly extract multiple morphometric attributes from features and allow statistical analysis of their morphology. While most of the progress and development on semi-automated geomorphology has occurred for subaerial or

* Corresponding author at: School of Biological, Earth and Environmental Sciences, University College Cork, Ireland.
E-mail address: rarosio@ucc.ie (R. Arosio).

https://doi.org/10.1016/j.geomorph.2024.109227
Received 15 December 2023; Received in revised form 22 April 2024; Accepted 23 April 2024
Available online 30 April 2024

planetary studies (e.g. Saha et al., 2011; Eisank et al., 2014; Roux et al., 2015; Gilbert et al., 2016; Foroutan and Zimbelman, 2017; Palafox et al., 2017), some researchers have developed methods to identify and occasionally also to characterise specific marine landforms, including seamounts (Hillier and Watts, 2004; Hillier, 2008; Wessel, 2016), drumlins (Saha and Van Landeghem, 2021), pockmarks (Andrews et al., 2010; Gafeira et al., 2012, 2018), subaqueous dunes (Di Stefano and Mayer, 2018; Summers et al., 2021; Lebrec et al., 2022) and coral mounds (Huvenne et al., 2003; De Clippele et al., 2017; Diesing and Thorsnes, 2018; Jarna et al., 2019).

Overall, semi-automated landform recognition from DEMs can be reduced to two separate conceptual procedures: (1) a landform is conceived as a negative or positive enclosed topographic relief; (2) a landform is conceived by its building blocks, or elementary facets (e.g. a sandwave is composed by a ridge, sides and a footslope), the facets can be identified automatically and then grouped to form the delineation of the landform. This latter method can produce accurate results (Di Stefano and Mayer, 2018; Sărășan et al., 2019; Cassol et al., 2021) but requires the careful implementation of a semantic procedure to "reassemble" the facets to form single complete landforms, which can be problematic in polygenetic or rough terrains. The identification of features' boundaries with method (1) can be carried out in different ways. The simplest methodology utilises contours to find confined landforms, where the most external closed contour of a set of contained closed contours is identified as the boundary of a feature. This method underestimates the size of features on sloping terrains and requires further mathematical analysis to refine the identification of the best contour (e.g. associated with break of slope (Wessel, 1998; Panagiotakis and Kokinou, 2017)). Several authors have relied on DEM derivatives such as curvature and aspect to identify the break of slope and hence features' boundaries (Grosse et al., 2012; Yu et al., 2015; Jorge and Brennand, 2017). However, this procedure is complicated by the fact that slope inflexions are inconsistent and can occur within the features (creating spurious delineations), and especially in marine environments, slope curvature can be minimal and disturbed by data acquisition artefacts. An alternative solution, extensively used by researchers working on seamounts, is to use mathematic filters to remove the wavelength of the topography underlying the landforms, thus ideally creating a resultant "de-trended" surface where positive relief is constituted only by the features to be mapped (Hillier and Watts, 2004; Hillier and Smith, 2008; Wessel, 1998, 2016). This method is fast and efficient but constrained by the subjective choice of filter size. In summary, no semi-automated method completely surpasses the other in flexibility, performance or user-friendliness. Moreover, some of these methods require access to specialist and expensive licensed software (e.g. Trimble eCognition), or assume at least some programming knowledge, and all of them are specifically tailored to the mapping of one particular landform type. While some existing toolboxes do provide complex systems to calculate morphological attributes of features (e.g. Huang et al., 2023), to our knowledge a flexible toolbox that provides the user with different methods for the mapping of confined landforms is absent.

We present therefore the Confined Morphologies Mapping (CoMMa) toolbox, a user-friendly ArcGIS Python Toolbox expressly created for semi-automated morphology mapping and that includes a selection of tools for the delineation and description of enclosed features on a DEM, either negative or positive. The delineation procedures consider the features as enclosed topographic relief and combine techniques of DEM filtering, contour definition or facets assemblage (Method 1 and 2 respectively, as described above) to provide a flexible and widely applicable solution to feature extraction. The backbone of the CoMMa Toolbox is based on the ESRI® ArcMap-based BGS Seabed Mapping Toolbox, which was originally developed to delineate pockmarks (Gafeira et al. (2012), never publicly released), but presents many additional features and more flexibility. The CoMMa Toolbox was developed for ESRI® ArcGIS Pro, which is arguably becoming one of the most common geographic information system (GIS) software programs in modern universities and specialised institutions, permitting users to work in a familiar environment. It does not require sophisticated GIS or programming skills and it is furnished with a thorough documentation that guides the user in the application of the toolbox. The toolbox still requires some expert knowledge and customised inputs from the user, but they are limited to identifying the best parameters for optimal recovery of the landforms of interest. The parametrisation allows replicability between different datasets and users, improving spatial or temporal comparisons (e.g. quantification of seabed changes over time). Mapping can be undertaken on any DEM dataset, pixel resolution, feature dimensions, and geological settings. Finally, reliable and repeatable morphological characterization can be carried out with only a fraction of the time and effort required using manual digitisation. While the Toolbox was created for a marine application, it may be employed to analyse elevation models of any provenance, including terrestrial and extra-terrestrial DEMs.

In this paper, we describe the features and applicability of the CoMMa Toolbox, compare both qualitatively and quantitatively its accuracy to a set of manually digitised geomorphology maps and discuss the potential of its general use in geomorphological mapping.

2. The CoMMa Toolbox

The CoMMa Toolbox is made up of individual Python scripts that use

Table 1
List of tools contained in the CoMMa Toolbox.

Toolbox	Toolset	Tool	Description
CoMMa Data Preparation	Local topographic Position (LTP) derivatives	Mean LTPs	Local topographic position index metrics based on the absolute and relative mean of the neighbourhood
		Median LTPs	Local topographic position index metrics based on the absolute and relative median of the neighbourhood
	Pre-processing tools	Smoothing filters	A series of standard filters used to smooth the DEM and remove noise and artefacts.
		Fencing	This tool creates an artificial containing fence at the boundary of the DEM, preventing the Fill algorithm from spilling out and thus permitting the delineation of landforms that are at the boundary. It has to be used in conjunction with the Filter and clip tool
		Filter and Clip	This tool removes the flat or featureless areas in the DEM and preserves areas of the seabed where the features are more likely to occur. The application of this tool is particularly useful to remove the effects of broad scale topography on Fill-based delineations.
CoMMa Delineation		Boundary-based delineation	Delineates confined landforms using a Fill algorithm on a DEM or a DEM LTP. Parameters can be modified to adjust for the height and width of the landforms of interest.
		Elements-based delineation	Delineates confined landforms using the Geomorphons algorithm on a DEM or a DEM derivative. Parameters can be modified to adjust for the height and width of the landforms of interest.
CoMMa Description		Basic descriptors	Calculates a series of basic geometrical and statistical attributes for each shape contained in the delineation shapefile.
		Texture descriptors	Calculates a series of basic textural attributes for each shape contained in the delineation shapefile.
		Volume descriptors	Calculates the volume and more accurately the height for each shape contained in the delineation shapefile.

a suite of embedded ArcGIS Pro geoprocessing tools and do not require the installation of any new Python package. The toolbox contains three independent blocks of tools (Table 1), which take the users through a series of concatenated steps that lead to a landforms map:

1. several pre-processing tools to remove artefacts from data and/or create DEM derivatives for landform delineation (CoMMa Data Preparation);
2. two landform delineation tools (Method 1 and 2 in the Introduction) to isolate the features of interest from the data (CoMMa Delineation);
3. three description tools to characterise each feature calculating individual parameters and attributes (CoMMa Description).

In the following section we offer a succinct description of each tool, sufficient for the scope of this paper, however the reader is referred to the GitHub release page (Arosio and Gafeira, 2023) or the Supplementary Material for a more detailed and illustrated User Guide to the use of the toolbox.

2.1. Data preparation tools

DEMs obtained from multibeam echosounder (MBES) data or other geophysical and optical instruments (e.g. Lidar, satellites, photogrammetry, 3D seismics etc.) may be affected by artefacts that can hinder a correct delineation of the features of interest, for example, corrugation in multibeam echosounder data caused by tidal shifts in line overlap or other vessel motion-related artefacts. A selection of basic filtering algorithms (mean, median and low-pass 3×3 or 5×5) has been provided as a first pre-processing package. These smoothing filters should at least partly correct the data, although they will also subdue the real signal proportionally to their respective aggressiveness.

Bathymetry DEMs might be sufficient to isolate landforms when the general seabed is otherwise flat, however, this is often not the case, and the interference of sloping topography or other underlying large-scale landforms can distort the signal of the targets. To address this issue mathematical operations can be applied to the DEM data to isolate a specific wavelength thought to best represent the feature of interest. Detrending techniques and other Local Topographic Position (LTP) metrics are common approaches in geomorphometric studies (De Reu et al., 2013; Wessel, 2016 and references within). LTP metrics quantify how elevated or low-lying a site is relative to the local topographic variability, creating a scale-dependent measurement that varies depending on the size of the neighbouring area to which the elevation is being compared (Lindsay et al., 2015). In marine studies, especially applied to habitat mapping, the bathymetric position index (BPI, originally topographic position index, TPI, in Weiss (2001)) is arguably the most applied absolute LTP (Harris et al., 2014; Walbridge et al., 2018). However, this is not because BPI is the most robust method - other derivatives have been shown to provide better results (see for example Wessel, 1998; Hillier and Smith, 2008; De Reu et al., 2013; Newman et al., 2018), but because BPI is often the only known or readily available LTP to the marine community (e.g. on QGIS or ArcGIS). CoMMa Data Preparation addresses this problem providing the user with a selection of derivatives that can complement the bathymetry at the delineation stage. The choice includes relative and absolute Median and Mean-derived LTP metrics; the description of each derivative is given in Table 2, while a more detailed account of their application is given in the User Guide. Other LTPs can be used at the delineation stage (e.g. Elevation Percentile (EP) (Newman et al., 2018), Relative Deviation from Mean Value (RDMV) (Lecours, 2017)), but will have to be calculated with other toolboxes.

The basic CoMMa Delineation process relies on a Fill algorithm that creates a cast of the seabed relief. Consequently, the CoMMa Toolbox provides a "Fencing" tool, which creates an artificial containing barrier around the perimeter of the DEM, preventing the Fill algorithm from spilling out and thus allowing the delineation of landforms that are only partially represented at the boundary of the dataset. The "Fencing" tool must be used in conjunction with the "Filter and Clip" tool, as holes must be created in the dataset to allow for the outflow and avoid a total flooding of the surface.

The "Filter and Clip" tool uses both High and Low Pass filters to identify areas of high rugosity on the bathymetry (where landforms are present) and then clips these areas from the original DEM. The "Filter and Clip" tool can be used ahead of delineations applied to bathymetry, effectively creating holes in the dataset that prevent the Fill algorithm to "flood" the large-scale topographical signal, thus capturing smaller, nested morphologies. While it is useful with original bathymetry DEM, it can be also applied to LTPs to avoid noisy delineations or reduce processing time.

Table 2
List of LTPs calculated by the CoMMa Toolbox.

Name	Description	Equation	Reference
Bathymetry Position Index (BPI)	BPI measures the vertical position of a pixel relative to the mean elevation (μ) of a user-defined neighbourhood.	$Z_0 - \mu$	Lundblad et al. (2006)
Deviation from mean elevation (DEV)	DEV measures the vertical position relative to the neighbourhood mean elevation (μ), but also normalizes by the standard deviation (σ) of the neighbourhood elevation distribution, effectively expressing local topographic position as a z-score.	$\frac{(Z_0 - \mu)}{\sigma}$	De Reu et al. (2013)
Median Bathymetry Position Index (M-BPI)	M-BPI measures the vertical position of a pixel relative to the median elevation (M) of a user-defined neighbourhood.	$Z_0 - M$	
Minimum Median Bathymetry Position Index (minM-BPI)	minM-BPI first calculates a minimum value surface (Zmin) running a convolution for a window defined as 1/4 of a user-defined neighbourhood. Subsequently it measures the M-BPI of the minimised surface.	$Z_0 - Z_{min} - M$	Adam et al. (2005)
Maximum Median Bathymetry Position Index (maxM-BPI)	maxM-BPI first calculates a maximum value surface (Zmax) running a convolution for a window defined as 1/4 of a user-defined neighbourhood. Subsequently it measures the M-BPI of the maximised surface.	$Z_0 + Z_{max} - M$	modified after Adam et al. (2005)
Directional Median Bathymetry Position Index (dirM-BPI)	dirM-BPI divides a given filter circle into N "bow tie" sectors, allocates data points inside the filter circle to each sector based on their relative position within the circle, estimates a median for each sector, and returns the lowest of these N medians.	$Z_0 - Mdir$	modified after Kim and Wessel (2008)

2.2. Landform delineation tools

CoMMa features both a "Boundary-based" and an "Elements-based" delineation tool, which cover the two conceptual procedures described in the introduction. The standard "Boundary-based" delineation takes

advantage of the hydrological algorithm "Fill" (ArcGIS Pro Spatial Analyst), filling up positive or negative enclosed relief in a DEM and subtracting the original unfilled layer, creating effectively separate "moulds" of potential features of interest (Gafeira et al., 2018). An alternative delineation can however be achieved applying the tool to an LTP obtained at the pre-processing stage; in this case the delineation will consist of a reclassification of the raster based on the thresholds inserted by the user.

The second delineation tool, "Elements-based delineation", relies on land surface units created by the *geomorphons* tool (Jasiewicz and Stepinski, 2013). *Geomorphons* compares the elevation of a focus pixel with the surrounding area utilising an 8-tuple pattern of the visibility neighbourhood. The 498 unique *geomorphon* patterns that can be produced are then grouped and reduced to 10 common landform elements describing the local surface shape (e.g. peak, ridge, pit etc.). The Elements-based delineation merges a selection of these elements established by the user, and then converts them into polygons (in a similar fashion to Di Stefano and Mayer (2018) or Sărășan et al. (2019)). Once again, the tool can be applied on either the simple bathymetry or an LTP; moreover, it does not require a Vertical Cutoff, but an "activation" slope that *geomorphons* will apply to discern flat from sloping pixel neighbours.

Several input variables must be defined to run these tools; these are the Vertical Cutoff, Minimum Vertical Threshold, Minimum Width, Minimum Width/Length Ratio and Buffer Distance (Fig. 1). The Vertical Cutoff is only required for the "Boundary-based delineation" and defines the contour line that will be identified as the feature's boundary. If the delineation is based exclusively on the input DEM, the Vertical Cutoff is applied to the raster resulting from the subtraction of the filled input DEM and the input DEM, where pixels with positive values indicate areas that have been filled by the algorithm. Whereas, if a derivative is also provided, such as an LTP layer, the Vertical Cutoff will be the minimum LTP raster value above which a pixel will be reclassified as a feature. This variable is always a positive (as for the delineation of negative feature, the input DEM is inverted), Rational number, normally approaching but not equal to zero (e.g. 0.2); however, the optimal number must be established by the user by trial-and-error. The Buffer Distance is meant to compensate for the Vertical Cutoff being greater than zero (Fig. 1), which often means that the periphery of features is not completely included (see Documentation in the GitHub repository for more information). The Minimum Vertical Threshold (i.e. vertical relief feature), Minimum Width, and Minimum Width/Length Ratio permit the user to define basic geometrical properties expected for the features, eliminating any delineation that does not possess the defined characteristics.

2.3. Landform description tools

CoMMa includes three landform description tools that can be run independently from one another and in any order. The "Basic descriptors" tool (Table 3) calculates a series of geomorphometric parameters for each polygon feature, ranging from shape metrics to zonal statistics of derivatives. Optionally, this tool allows the user to confront the delineation with land surface units calculated by geomorphons, measuring the percentage area of each land surface unit, and counting the number of peaks (if positive morphologies) or pits (if negative morphologies) contained within each polygon feature. These measurements can give useful indication of the complexity of the mapped landforms. The "Texture descriptors" tool adds a few additional metrics that describe the quality of the surface, including zonal vector ruggedness measurement, aspect variability index and optionally backscatter statistics (Table 3). Finally, the "Volume descriptor" calculates the best approximation of the vertical relief and the volume of the feature. These calculations are based on the Cookie Cutter method proposed by Smith et al. (2009) and are performed on a feature-by-feature basis, slowing down considerably the processing time. The function of these tools is two-fold. The first purpose is discriminatory; after landforms are delineated and vectorised, the result might still be including morphologies that do not belong to the class that the user intends to map. The attributes calculated may allow then the selection and removal of morphologies hinging on attribute-based rules. The second function is analytical, allowing for statistical examination of the mapped landform population. In line with the objective of a flexible solution, CoMMa's attribute choice was defined by usefulness and applicability to a broad range of marine geomorphometry and habitat mapping studies, without a focus on any particular landform. CoMMa users can also rely on other published description toolboxes (e.g. ACME2 (Li et al., 2024), GA-SaMMT (Huang et al., 2023) or MORVOLC (Grosse et al., 2012)) for more targeted analyses.

3. Tool assessment methods

To assess the accuracy of the semi-automated delineation with absolute measurements, we ran tests in a controlled environment with a priori knowledge of its structure. Structural knowledge can be attained with the use of synthetic DEMs, i.e. artificial surfaces which are created by the sum of different "strata" whose thicknesses (heights) are known at any (x,y) location (Hillier and Smith, 2012; Hillier et al., 2015b). In this case, the height Z_T of a simple synthetic DEM at any (x,y) (i.e. a pixel in a raster) was composed of:

$$Z_T = Z_B + Z_L + Z_N \quad (1)$$

where Z_B is the height component of a background surface (the underlying seabed landscape), Z_L is the height component of the landform set,

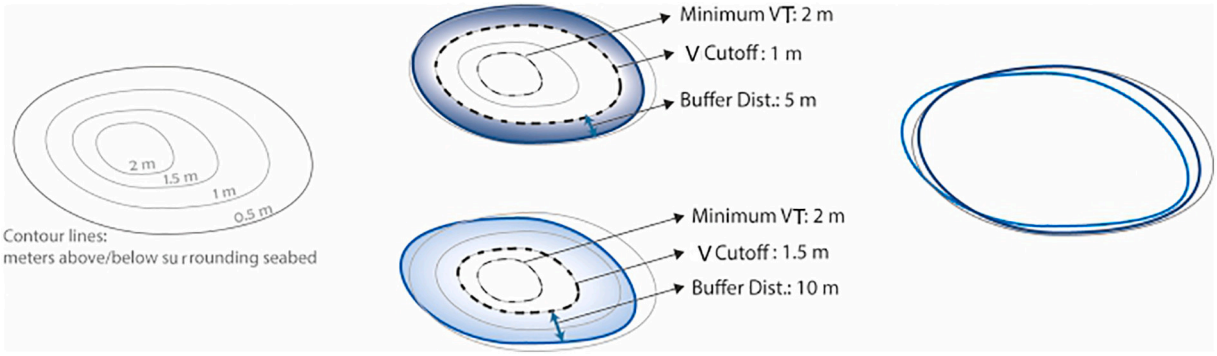

Fig. 1. Visual representation of the parameters required for the automated delineation.

Table 3
List of attributes calculated by the Delineation tools (D Tool) and the three descriptor tools, Basic Descriptor (B Des), Texture Descriptor (T Des) and Volume Descriptor (V Des).

Attribute	Field name	Description	D Tool	B Des	T Des	V Des
Area	Area	The area of the polygon feature				
Perimeter	Perimeter	The perimeter of the polygon feature				
MBG width	MBG_Width	Width of the Minimum Bounding Geometry (rectangle) as calculated by the ArcGIS Pro tool				
MBG length	MBG_Length	Length of the Minimum Bounding Geometry (rectangle) as calculated by the ArcGIS Pro tool				
MBG width/length ratio	MBG_W_L	Ratio of MBG width and MBG length				
MBG main orientation	MBG_Orient	Orientation of the Minimum Bounding Geometry (rectangle) as calculated by the ArcGIS Pro tool				
Relief	Relief	The first calculated polygon feature height, based on the general fill of the bathymetry, it may give spurious numbers as it gets heights from areal fills instead of feature-focussed fills				
Minimum, mean and maximum slope	Slope_MIN; Slope_MAX; Slope_MEAN	The minimum, mean and maximum slope within the polygon feature				
Mean and maximum LDfG	LDfG_MAX; LDfG_MEAN	The mean and maximum local deviation from global median value within the polygon feature				
Minimum, mean and maximum depth	Depth_MIN; Depth_MAX; Depth_MEAN	The minimum, mean and maximum depth within the polygon feature				
Polsby-Popper test for circularity	PP_Score	Calculated as $4\pi \times Area/Perimeter^2$ (Cox, 1927)				
Convex hull area	Area_CH	Area of the Minimum Bounding Geometry (convex hull) as calculated by the ArcGIS Pro tool				
Convex hull-object area ratio	CH_Score	The ratio between the convex hull area (Area_CH) and the area of the polygon feature (Area)				
Dissection index	Dissect	The ratio of the maximum relative relief to maximum absolute relief $\frac{Depth_{MIN} - Depth_{MEAN}}{Depth_{MIN} - Depth_{MAX}}$				
Depth range	Depth_RAN	The difference between the maximum (Depth_MAX) and minimum (Depth_MIN) depth				
LDfG variance	LDfG_VAR	The variance of local deviation from global median value within the polygon feature				
LDfG quintile rank	QuLDfG_ran	Ranked quintiles of LDfG mean (mound belongs to one of the quintiles)				
Confinedrelief	Conf_R	The second calculated polygon feature height; this is extracted by first clipping the features, then filling the bathymetry, producing a "confined" vertical relief that can be sometimes an underestimation of the real height				
Geomorphons class percent	gm_peak; gm_ridg; gm_shou; gm_spur; gm_slop; gm_holl; gm_vall; gm_pit	Percentage area of different geomorphons land surface units contained within each polygon feature. Positive features will count % area of peaks, ridges, shoulders, spurs and optionally slopes. Negative features will count % areas of pits, valleys and hollows.				
Geomorphons peaks or pits number	peak_no; pit_no	The number of distinct peaks (if positive) or pits (if negative) within the polygon feature as calculated by the geomorphons layer. Peaks or pits composed of less than 4 pixels are not counted.				
Minimum, mean and maximum ruggedness	Rugg_MIN; Rugg_MAX; Rugg_MEAN	The minimum, mean and maximum ruggedness (as calculated in Sappington et al., 2007) within the polygon feature				
Minimum, mean and maximum AVI	Avi_MIN; Avi_MAX; Avi_MEAN	The minimum, mean and maximum aspect variability index (AVI) within the polygon feature (Nielsen et al., 2004)				
Minimum, mean and maximum backscatter	Bsc_MIN; Bsc_MAX; Bsc_MEAN	The minimum, mean and maximum multibeam echosounder backscatter value within the polygon feature				
Optimal relief	Optim_R	Last and best approximation of height. This number is calculated on a feature-by-feature basis on the isolated and detrended DEM of the feature.				
Volume	Volume	Volume of each polygon feature calculated using the CookieCutter method (Smith et al., 2009)				

and Z_N is the height component of eventual noise (e.g. artefacts or other landforms superimposing the basic seabed landscape) (Fig. 2B). In a (x, y) where the landforms and/or noise are absent, those height components will be equal to zero. Thus, the stratum Z_L in our synthetic DEM contains only elevation data of the landforms that we want to map. The knowledge of the "correct" morphology (e.g. height, width etc.) of a landform set permits a rigorous testing of the performance of a delineation method, and the calculation of absolute metrics of correctness and completeness (e.g. x% of all existing landforms of interest with H > z metres are mapped) (Hillier et al., 2015a, 2015b). Moreover, it permits an assessment of the filtering and filling technique used to manipulate the DEM, where the choice of parameters and thresholds would otherwise be subjective.

In this study, we tested the accuracy and efficacy of the delineation

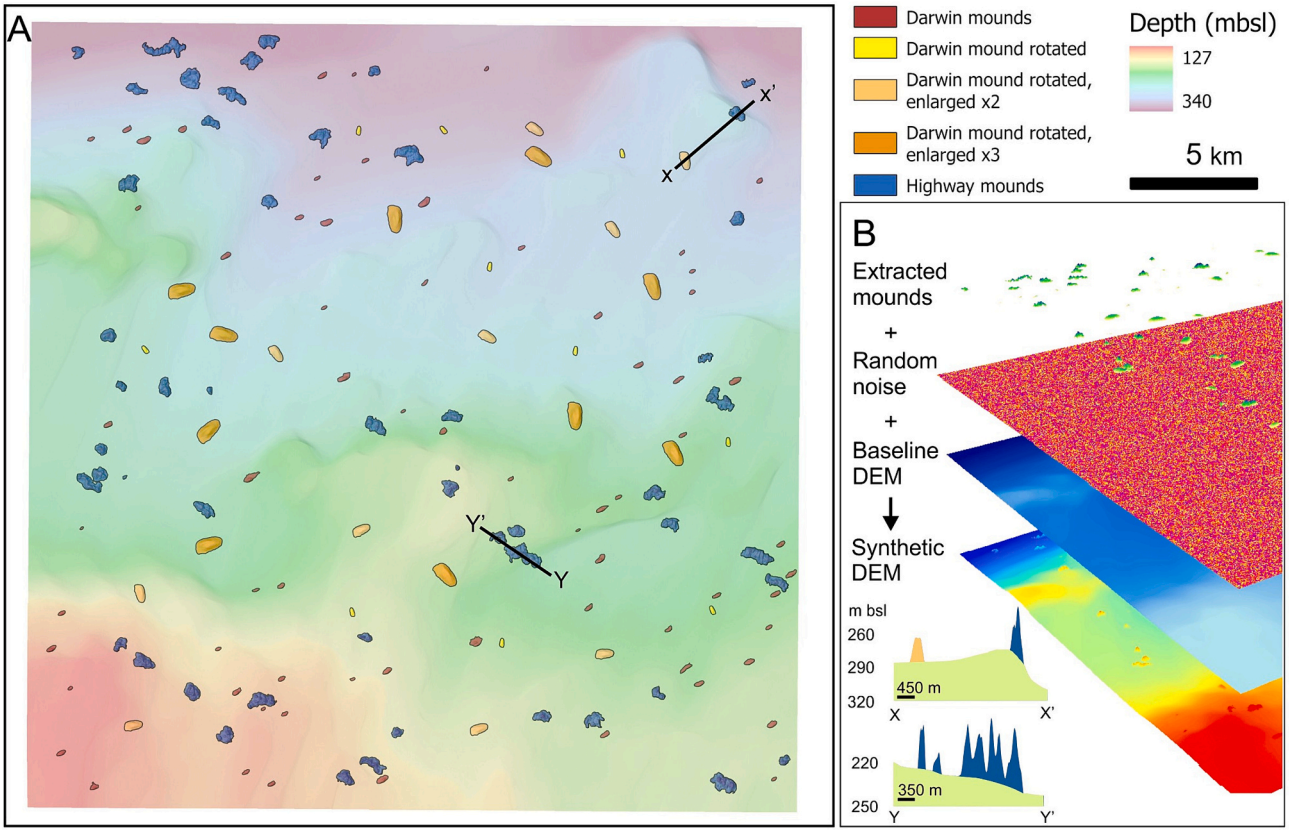

Fig. 2. Summary of the data utilised in this study. A) distribution of the mounds from the two original datasets and replicated mounds. B) schematic representation of the construction of the synthetic DEM. X-X′ and Y-Y′ show two example profiles of the mounds and underlying baseline bathymetry.

tools within CoMMa Toolbox by qualitatively and quantitatively comparing the Toolbox outputs against the manual delineations produced by five geomorphologists, using a synthetic dataset (DEM) of 150 coral mounds.

3.1. Coral mound datasets

Two different MBES datasets containing cold-water coral mounds were harvested for the synthetic DEM creation, in order to include morphologically distinct features and better test the toolbox. Cold-water corals are coral species that do not live in symbiosis with algae, and hence are found beyond the photic zone in deep and dark parts of the world's ocean. Cold-water coral mounds are biogenic, long-lived morphostructures composed primarily by scleractinian cold-water corals and hemipelagic sediments that form complex deep-sea microhabitats found globally but specifically along the European-Atlantic margin (Conti et al., 2019). The first dataset is from Darwin Mounds, northern Rockall Trough, NE Atlantic, and the second is from Highway Mounds, Blake Plateau, East Florida. The Darwin Mounds MBES data was collected in 2011 as part of the RRS James Cook Cruise 60 (Huvenne, 2011). An EM2000 MBES was attached to an Autonomous Underwater Vehicle (AUV) and operated at 100 m height above the seafloor to create a bathymetric dataset with a 2 m/pixel resolution. The Darwin Mounds cold-water coral mounds are relatively small (up to 75 m in width and 5 m in height), simple, ellipsoidal knolls, and are found isolated or grouped between 900 and 1060 m water depth. The main coral species found growing on the mounds is *Lophelia pertusa* (also referred to as *Desmophullum pertusum* sensu Addamo et al. (2016)), but the coral *Madrepora oculata* has also been recorded (Wheeler et al., 2008; Huvenne et al., 2009).

The Highway Mounds were mapped during the *Windows to the Deep* 2018 and 2019 expeditions by NOAA Ship Okeanos Explorer using a Kongsberg EM 302 sonar operating at a frequency of 30 kHz (Cantwell et al., 2019, 2020). The bathymetry data was downloaded from NOAA's NCEI Bathymetry Data Viewer (https://maps.ngdc.noaa.gov/viewers/bathymetry/) and gridded at a resolution of 30 m/pixel. The Highway Mounds include much bigger features than the Darwin Mounds, with landforms reaching more than 1.2 km in length and up to 65 m in height; they are also morphologically more complex, showing a rugged topography made of knobs and pits and an irregular perimeter. The summits of these mounds are covered in a high percentage of *Lophelia pertusa* and patches of *Madrepora oculata* corals (Cantwell et al., 2019).

3.2. Production of the synthetic DEM

The procedure for synthetic DEM creation was based on the one proposed by Hillier and Smith (2012) for their analysis of drumlins, and modified where required for our case study. Firstly, a background DEM was obtained by cutting a portion of existing seabed where no coral mounds are present but that possesses general physiography compatible with locations where coral mounds naturally occur. In this case, we cut, gridded at 5 m/pixel resolution and smoothed (Low Pass filter) a square of 30.5 × 30.5 km from the northern Porcupine Bank, Ireland (obtained from www.infomar.ie). Secondly, a raster of the same size and pixel resolution as the background DEM containing random noise with z values of ±0.2 m was generated. Thirdly, the real coral mound features were clipped from their original bathymetries (see Section 3.1) using the CoMMa Toolbox and geographically shifted to match with the position of the background DEM. A total of 68 mounds were obtained from the Darwin dataset, while the Highway data contributed to 52 mounds; due to the considerable difference in feature size between the two mound groups, the Darwin mounds were slightly expanded to make them more comparable with the dimensions of the Highway mounds. Another 30 mounds were obtained by copying, enlarging (x1, x2 and x3 in groups of

10), shifting and rotating one of the mounds from the Darwin dataset (Fig. 2A). These replicate sets were created to test the ability of semi-automated or manual mappers to consistently delineate identical features in different orientations. A total of 150 synthetic mounds were thus produced; these mound shapes, independently from the effective correctness of the original extraction and notwithstanding the transformations applied, were adopted as "true forms" and used as baseline for different mapping approaches comparison. Before joining the "true form" mounds to the background DEM and noise, the mounds were re-gridded at 5 m/pixel resolution and each feature was catalogued by giving a unique ID, and their shape and texture metrics were calculated using the tools in the "CoMMa Description" toolset. These attributes act as the absolute measurements against which the extraction techniques are tested. Finally, the mounds were randomly placed on the baseline DEM to create a distribution unrelated to their original relative locations. The different baseline DEM was chosen for its gentle undulation, different from the mostly flat seabed of the two datasets with coral mounds, which complicates the semi-automated extraction. These modifications and the superimposition to a different baseline topography should nullify any link between the original delineation parameters used to generate mounds and the synthetic DEM.

3.3. Manual and semi-automated mapping

Five manual mappers, all cold-water coral mounds experts with previous experience using GIS and manual digitisation of submarine landforms, were given a maximum time of 2 h to complete the manual digitisation of the mounds – i.e. positive relief, confined features, within the synthetic DEM. They were allowed to use any kind of DEM derivative as a visual support but asked to keep a fixed mapping scale at 1:10,000. The mappers were not aware of the total number of mounds and were not compelled to find them all. They were also asked to leave any comment and feedback on the difficulty of the task and their *modus operandi*.

Semi-automated mapping was carried out by the first author utilising the filtering and delineation tools available in the CoMMa Toolbox to obtain the best possible delineation. As for the manual mappers, a maximum time of 2 h was allowed to reach the final result and included the time required to create the LTPs.

3.4. Accuracy evaluation metrics

Several metrics were adopted to assess the accuracy of the results. Firstly, the areal correspondence between mapped and true form was measured, and the percentage of concurred, missed and in excess mound area was calculated. A summary index for areal "goodness-of-fit" (GoF) based on the equation proposed by Hargrove et al. (2006) was also calculated. A set of two metrics, the normalised Hausdorff distance (HD) (Rockafellar and Wets, 2004) and Pratt evaluation metric (PEM) (Abdou and Pratt, 1979), were employed to gauge the structural similarity of the delineations obtained with the CoMMa tools and by expert mappers against the real perimeters of the mounds. HD essentially measures the maximum distance between any point on the real perimeters and its nearest point on the delineation, and vice-versa. PEM instead represents the deviation of a mapped perimeter point from the true perimeter. These figures were calculated in Python transforming the delineations into *numpy* arrays of 0 and 1, where ones correspond to delineations and zeroes to *NaN*. HD was obtained via the algorithm built in the package *scikit-image.metrics*, and then normalizing the result by dividing by the diagonal distance across the envelope of the combined arrays, with 0 meaning perfect overlap and 1 highest distance. PEM was instead calculated by adapting the MATLAB algorithm by Bhadouria (2023) in Python, where 0 represents least correlation and 100 perfect matches.

The final metric is the percentage error (EP) obtained from the comparison between a selection of "CoMMa Description" parameters of predicted against real mounds, where lower errors would indicate more accurate delineations.

4. Results

A summary of the results of the statistical analysis are presented in Table 4, while the complete tables are provided in the Supplementary Material (Tables S1, S2, S3 and S4). In this section, the delineations of the manual mappers and CoMMa Toolbox are described separately, and then their quality is discussed against the "true form" mounds. Table 4 shows that in a few cases extra mounds were mapped: these are small spurs protruding from the main "body" of the more complex mounds which have been misinterpreted as separate features. These extra mounds have been grouped with the "main body" for the calculation of areal correspondence and structural similarity metrics, but could not be included into the mean EP of the attributes.

Table 4
Summary of the accuracy metrics for the results of the five manual mappers and the best CoMMa delineation. GoF is the Goodness of Fit measurement based on the areal correspondence. †Mean and standard deviation calculated only for the mounds mapped by all (61). The mean EP was calculated using the following attributes: Optim_R, Volume, Conf_R, Area, Perimeter, MBG_Width, MBG_Length, MBG_W_L, MBG_Orient, Area_CH, CH_Score, Dissect, Depth_RAN and PP_Score. The Standard deviation of the replicates is an average of the Standard deviation for all the replicated mounds.

		True form	Mapper 1	Mapper 2	Mapper 3	Mapper 4	Mapper 5	CoMMa best
Mounds count		150	134	142	151	78	151	153
Total area (km^2)		25.86	20.6	22.8	25.2	20.8	26.4	23.2
GoF			0.821	0.771	0.827	0.877	0.922	0.853
Area	Concurred		77.30 %	82.90 %	88.00 %	75.20 %	94.70 %	89.20 %
	Missed		21.40 %	14.30 %	7.20 %	22.00 %	1.70 %	10.40 %
	In excess		1.30 %	2.90 %	4.80 %	2.90 %	3.60 %	0.40 %
EP (attributes)	Mean		8.98 %	10.98 %	7.42 %	5.56 %	3.10 %	8.06 %
	Mean†		4.89 %	9.68 %	4.80 %	5.21 %	2.30 %	5.93 %
Hausdorff distance	Mean		0.38	0.39	0.36	0.34	0.34	0.38
	Std		0.13	0.16	0.13	0.14	0.15	0.12
	Mean†		0.34	0.35	0.33	0.33	0.32	0.35
	Std†		0.13	0.17	0.13	0.14	0.14	0.13
Pratt evaluation metric	Mean		3.57	2.84	3.42	4.09	6.19	4.93
	Std		2.62	2.21	2.01	2.47	2.85	4.55
	Mean†		4.34	2.95	3.75	4.12	5.89	6.01
	Std†		2.61	2.42	1.98	2.64	2.32	4.88
Replicates	HD Std		0.10	0.10	0.07	0.10	0.12	0.08
	EP Std		4.15	7.71	1.92	2.39	0.82	1.27

4.1. Manual mapping results

All the mappers used the entire 2-h period allotted to complete the digitisation, apart from Mapper 3 who required only 1 h and 8 min. Mappers 2, 3 and 4 relied solely on a hillshade or slope layer (multidirectional only for Mapper 3) to guide their delineation, while Mappers 1 and 5 utilised a combination of different derivatives including slope, slope isolines, plan curvature and hillshades to help them find the correct boundaries of the features. Unsurprisingly, all the mappers complained about sore wrists and fingers from prolonged mouse clicking and Mapper 1 observed decreasing personal performance as time went by. However, this is not clearly observable in the evaluation metrics (see Supplementary Material Fig. S4) and in fact, performance deterioration by time for human mappers appears to be insignificant in this exercise, although some decline might be present for Mappers 2 and 4 (Supplementary Material Figs. S6 and S10). Due to the different methodologies and styles, it is perhaps not surprising that the results of the manual mapping exercise show a wide range of accuracies and completeness (Table 4). None of the mappers were able to find the correct number of mounds, although almost all got very close to it. Mappers 1, 2 and 3 performed similarly, getting very close to the total number of mounds (134, 142 and 151 respectively) and obtaining a correct coverage of about 80 % (GoF 0.806). Mapper 3 produced relatively better results than the other two, and this is especially reflected in the lower average EP related to attributes, ~7.4 % compared to a higher ~10 % between the other two mappers. Mapper 4 constitutes the outlier of this exercise: they mapped only 52 % of the dataset, missing the great majority of the small-sized mounds which they considered as bathymetric noise. Because of this outcome statistics calculated for Mapper 4 cannot be promptly compared to others. Hence Table 4 presents the evaluation metrics both for the entirety of the mound population mapped by each mapper, and those restricted only to the 61 mounds mapped by everyone. Mapper 4's results on the reduced dataset show very similar performance to Mapper 1, if only slightly superior. Finally, Mapper 5 clearly surpasses in accuracy and completeness all the other manual mappers, finding 151 mounds (i.e. delineating separately a spur from one large mound), correctly covering 95 % of the mound area (GoF 0.922). Accuracy scores are consistently superior all round, including PEM which is ~6.2 against an average of 3.8 for the other mappers, suggesting higher competence in finding exactly the right boundary.

4.2. CoMMa Toolbox outputs

With regards to the semi-automated mapping, the entire 2-h period was utilised to create several LTPs and test different combinations of input layers and parameters to obtain the best possible (in a visual sense) result. A total of seven delineations were produced but only the scores of the most accurate are presented in Table 4. The best delineation was obtained following this procedure: first, the LTP "Minimum Median" with a radius of 250 m was created and then cut using the "Filter and

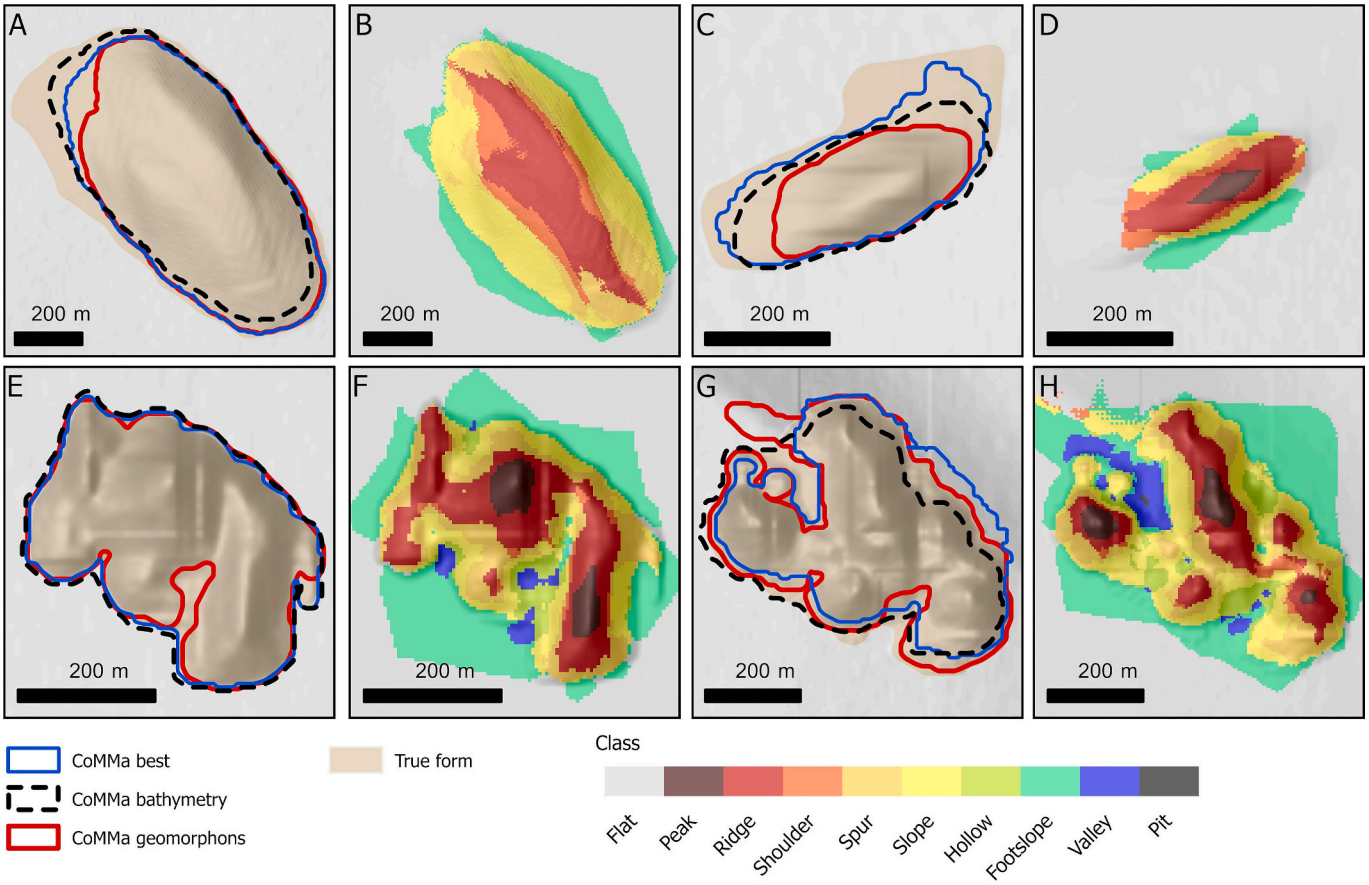

Fig. 3. Comparison of three CoMMa results for four representative mounds: CoMMa best (from the LTP minimum median 50, filter and clipped, as described in the text), CoMMa bathymetry, obtained applying the "Filter and clip" tool purely on bathymetry (filter threshold: 0.2 and buffer size of 150 m) and a "Fill-based delineation" (Cutoff value: 0.2; Minimum relief value: 1; Minimum Width (m): 20; Minimum W/L Ratio: 0.2; Buffer extent (m): 7.5); CoMMa geomorphons, obtained applying the in-built ArcGIS Pro *geomorphons* tool on a minimum median LTP with radius 400 m, and then a "Geomorphons-based delineation" (Including peaks, ridges, shoulders, spurs and slopes; Minimum relief value: 1; Minimum Width (m): 20; Minimum W/L Ratio: 0; Buffer extent (m): 10). Insets A, C, E and G show the delineation results against the real area of the mounds (true form, beige hillshade), while insets B, D, F and H show the geomorphons layer. Delineations and geomorphons layer are semi-transparent and superimposed on a multidirectional hillshade layer (z exaggeration x3). Mounds in A and C are from Darwin Mounds, while E and G are from Highway Mounds.

Clip" tool with a filter threshold of 0.3 and buffer size of 150 m. Secondly, the Boundary-based delineation tool was applied (Cutoff value: 0.3; Minimum relief value: 2; Minimum Width (m): 20; Minimum W/L Ratio: 0; Buffer extent (m): 2), where the best parameters were established heuristically and relying on the temporary outputs of the tool which the user can save in a folder (see the User Guide in the GitHub repository for more information). This process obtained 153 mounds (the extra 3 being separate "spurs"), a good concurred areal coverage at almost 90 % (GoF 0.853) and mean EP on attributes at ~8 %.

Figs. 3 and 4 show the comparison between the best CoMMa delineation and two other CoMMa results, one derived using the Boundary-based delineation solely on bathymetry, and the second obtained from the Elements-based delineation on an LTP (production details are given in the figure's caption). The small sample of mounds selected for the figures (also Figs. 5 and 6) does not show all the variations for the entirety of the population but it is representative of the range of results, showing in equal measure the morphologically different Darwin and Highway mounds, including the range of sizes, and the mapping styles of the different mappers. The reader can refer to the shapefiles in the Supplementary Material for a full assessment of the results. The Elements-based delineation is the least effective in this case, especially for Darwin mounds with gently sloping peripheral areas (e.g. Figs. 3A and C, 4C and E), which are not captured due to the influence of the "activation" slope parameter. The slope parameter we used is not sufficient to include the peripheries, but a lower slope parameter would have included in the delineation of much larger swaths of surrounding terrain causing instead "over-mapping". The bathymetry-based Boundary delineation provided generally good results, as clearly shown in Figs. 3 and 4, nonetheless overall it tended to underrepresent mound features compared to the LTP-derived results (e.g. Figs. 3C, 4A and E). The bathymetry delineation is however less affected by the underlying topography (e.g. Fig. 3G), which tends to influence LTP Boundary delineations because of the neighbourhood size (radius) used for the creation of the LTP itself. In particular, depending on the size of the radius features of a certain size will be optimally extracted to the detriment of other sizes (see Hillier (2008) for a more in-depth discussion).

5. Discussion

5.1. Manual vs CoMMa comparison

An initial, cursory look at Table 4 reveals that the best CoMMa delineation falls within the range of competence demonstrated by the expert manual mappers (see also Figs. 5 and 6), with scores comparable to Mappers 1 to 4, although it never reaches the performance of the best human-made delineation (Mapper 5). CoMMa's delineation tool achieves a good areal correspondence (GoF 0.853) with very little excess mapped (0.4 %) compared to any manual mappers (average 3.1 %), and additionally shows the highest PEM against Mappers 1–4 (~5 against a mean of ~3.5), indicating a better capacity to delineate very close to the correct perimeter. PEM is even higher - in fact, the highest among all delineations (~6 against a mean for all manual mappers of ~4.2), for the reduced dataset, which comprises almost exclusively the large units, mostly Highway Mounds. These results confirm, as discussed above, that the LTP-based delineation used is very effective for a specific range of feature dimensions, in this case the larger features.

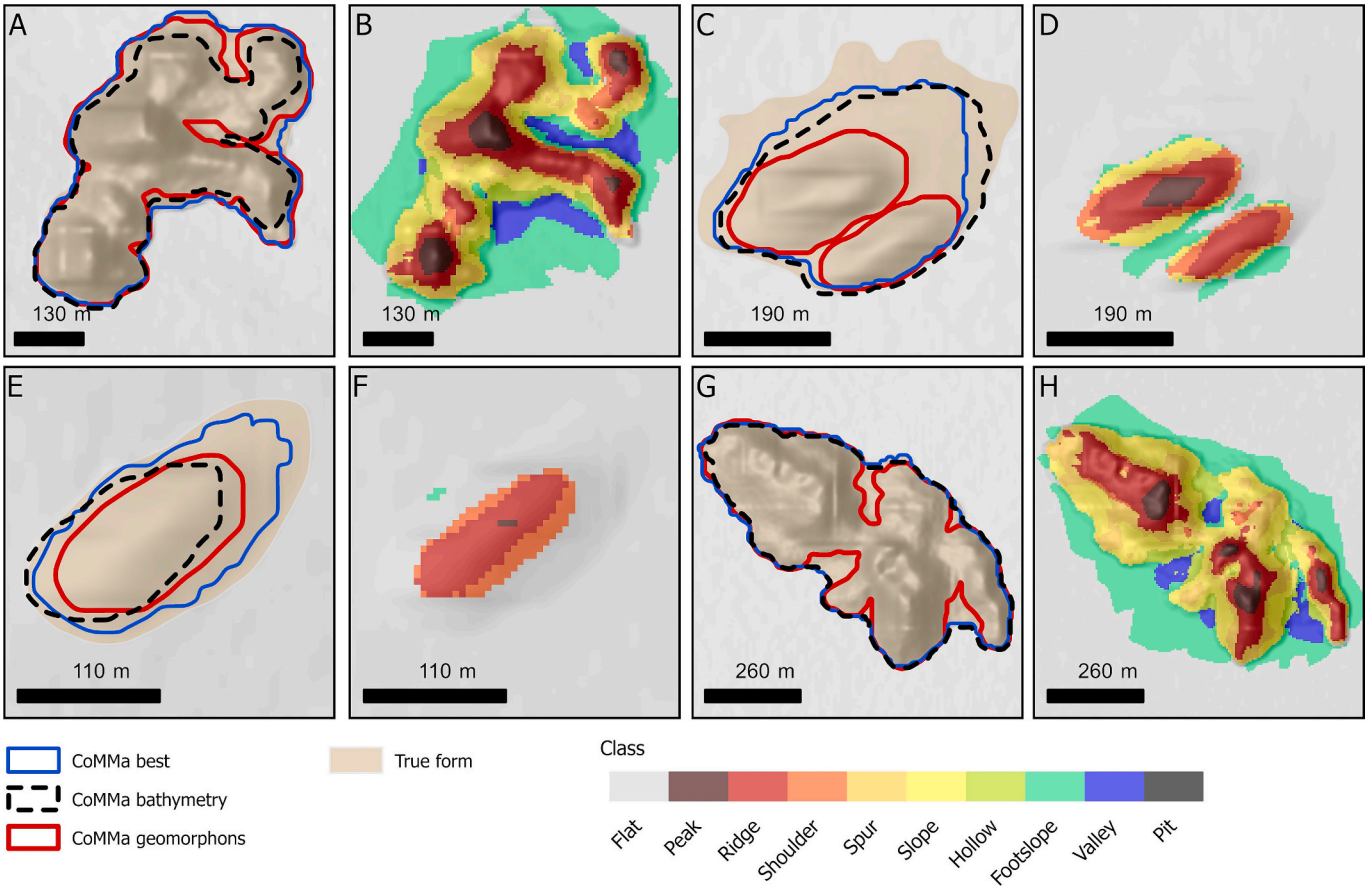

Fig. 4. Comparison of three CoMMa results for four additional representative mounds: CoMMa best, CoMMa bathymetry and CoMMa geomorphons (see the caption of Fig. 3 for the parameters used in their creation). Insets A, C, E and G show the delineation results against the real area of the mounds (true form, beige hillshade), while insets B, D, F and H show the geomorphons layer. Delineations and geomorphons layer are semi-transparent and superimposed on a multidirectional hillshade layer (z exaggeration x3). Mounds in A and G are from Highway Mounds, while C and E are from Darwin Mounds.

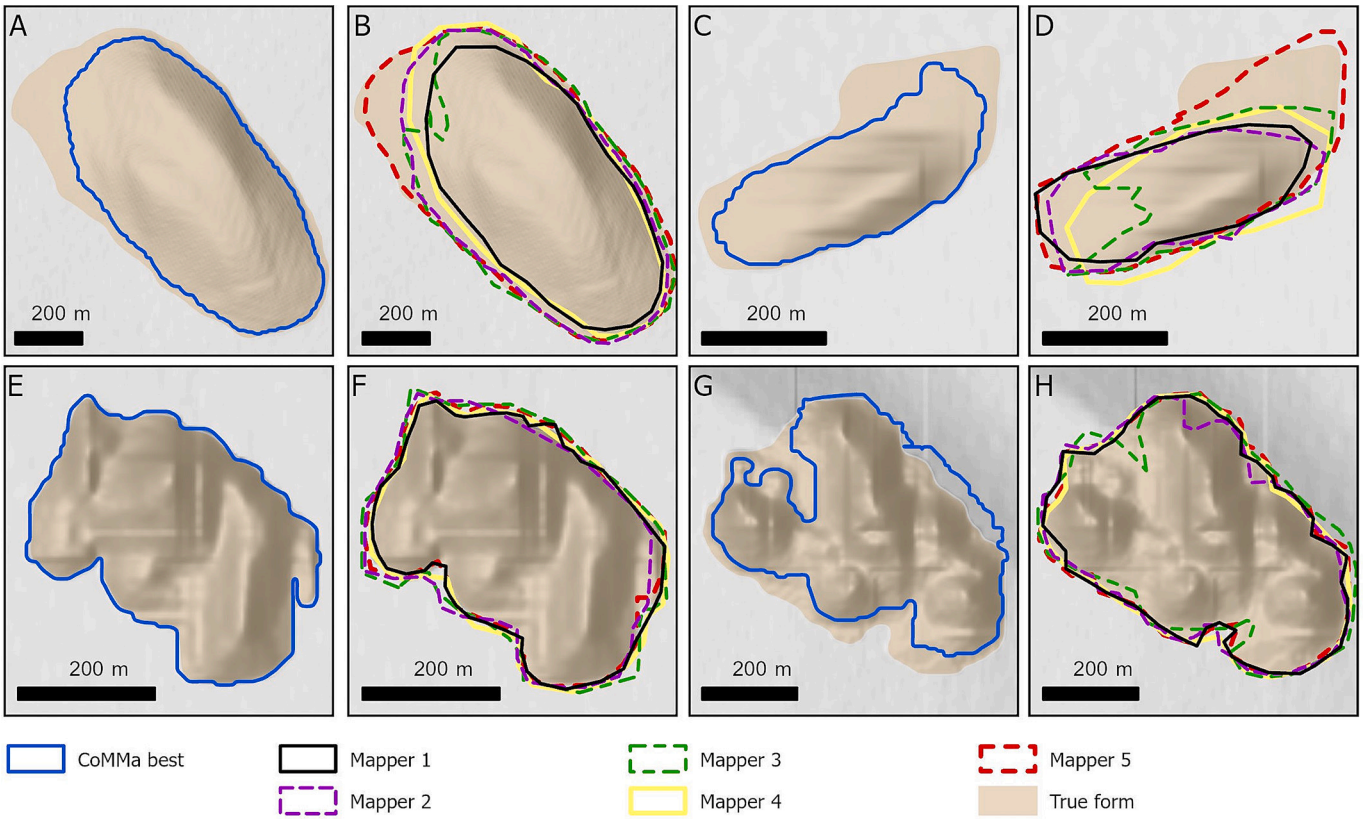

Fig. 5. Comparison of the best CoMMa results (A, C, E and G) with the delineations of the manual mappers (B, D, F and H) against the real area of the mounds (True form, beige hillshade). The mounds are the same as in Fig. 3. A and C are from Darwin Mounds, while E and G are from Highway Mounds. Delineations are superimposed on a multidirectional hillshade layer (z exaggeration x3).

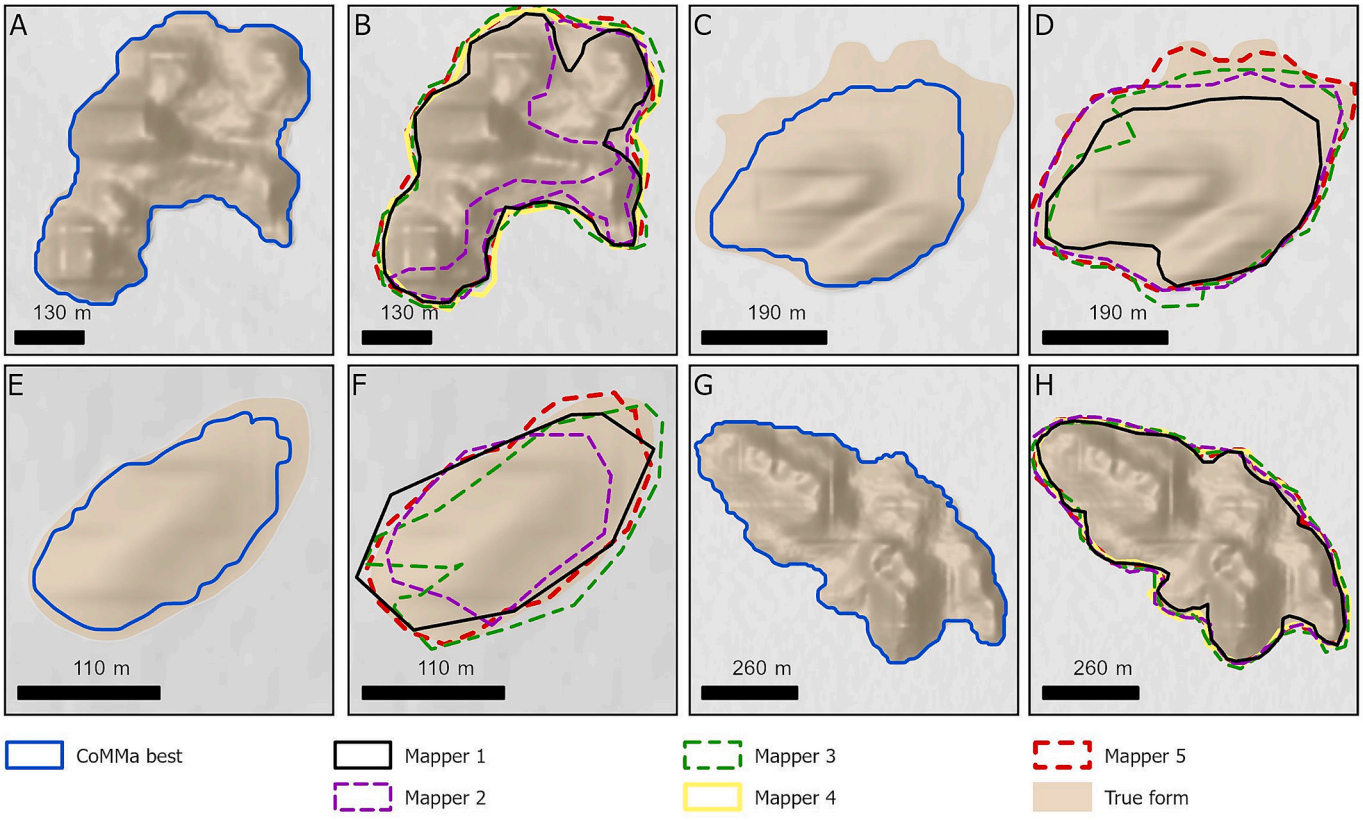

Fig. 6. Comparison of the best CoMMa results (A, C, E and G) with the delineations of the manual mappers (B, D, F and H) against the real area of the mounds (True form, beige hillshade). The mounds are the same as in Fig. 4. A and G are from Highway Mounds, while C and E are from Darwin Mounds. Delineations are superimposed on a multidirectional hillshade layer (z exaggeration x3).

When comparing the similarity of replicate delineations (i.e. Darwin Mounds rotated and/or enlarged), CoMMa does not seem to strongly outperform the manual mappers, but it aligns with the strongest mapper's results (Mapper 3 for HD and 5 for EP) and achieves consistently better results than Mappers 1,2 and 4 (Table 4). These results occur also for the bathymetry Boundary-based delineation (see Supplementary Material Table S1), confirming that the semi-automated procedure is influenced by rotations and displacement, as the direction of filtering for the LTP and the underlying topography will affect the extraction.

The best manual maps were produced by experts relying on multiple terrain derivatives to guide their delineations, and not only a single layer. Different forms of visual bias-induced errors, sometimes substantial, can be observed in the outputs of manual mappers. For example, in Fig. 5B and D Mapper 3 deviates from a regular curvilinear boundary to create indentations that are probably due to hillshade or pure slope bias (Smith and Wise, 2007; Scheiber et al., 2015) while in Fig. 6B Mapper 2 misrepresents a mound more than halving its size, which can be due to their use of a unidirectional hillshade. These abnormal deviations are absent in CoMMa's delineation, which is not affected by visual bias although care needs to be taken in the use of LTPs and the effect of underlying topography.

Within the framework of this exercise, we demonstrated that CoMMa delineation tools quickly provide the user with outputs comparable, if not superior, to most human mappers. In the 2-hours time limit given for this exercise, the CoMMa user was able to create and test seven different combinations of LTPs and delineation approaches and choose the best among them. The CoMMa user in this exercise was aware of the correct number of mounds. However, we argue that tool thresholds are inserted based on the general visual scanning of landform population dimensions, so it is unlikely for the toolbox to miss landforms with comparable size, and if the user correctly identifies the thresholds and delineation method, they should be able to capture all comparable features present on the dataset. It then follows that CoMMa Toolbox provides additional assistance in the identification of features that might be unnoticed on first visual inspections or manual delineations. Conversely, CoMMa's delineation tools are more prone than human mappers to create a surplus of delineations, most of them spurious. These will have to be filtered out either manually or relying on utilising the attributes (e.g. Area, Relief, W/L Ratio etc.).

The CoMMa Toolbox can be reliably used for morphometric calculations, for example, extraction of volumes, heights, orientations etc. CoMMa errors plot close to the average of all the mappers, at 8 %, (Fig. 7) and while this figure is not insignificant, it is instructive to see that only one mapper (Mapper 5) was able to consistently keep EPs below 5 %, suggesting that manual maps, which are often used as golden standards, can carry this magnitude of error.

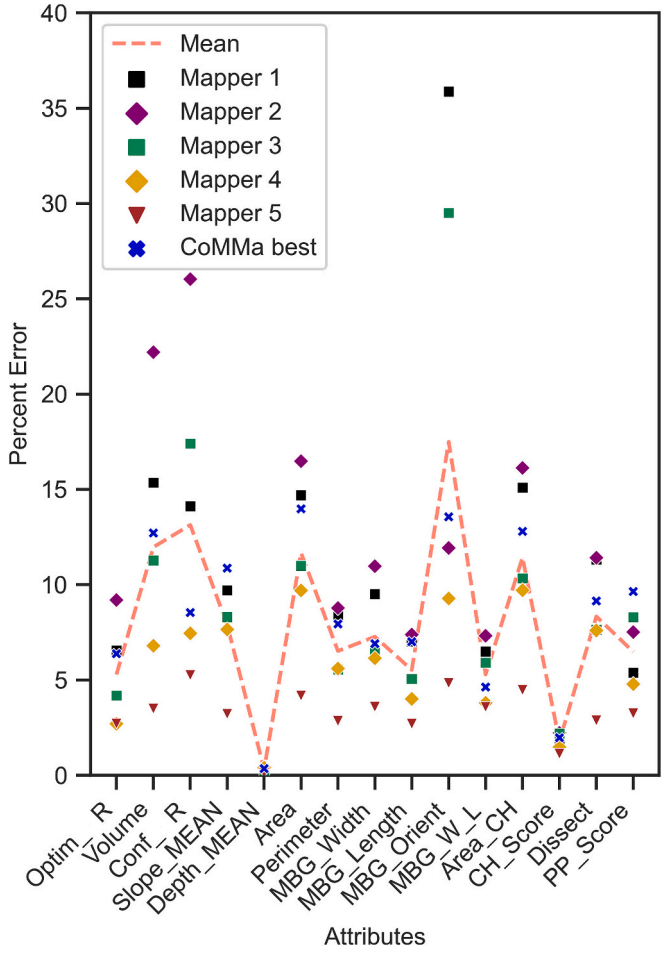

Fig. 7. Mean Percentage Error on a series of calculated attributes for the six delineations of this study.

5.2. CoMMa in marine landform extraction

In this study we have presented a single mapping example applied to coral mounds; however, CoMMa can be readily adopted for several types of enclosed landform, and a few studies have already shown its potential for bedrock outcrops, drumlins and other biogenic mounds (Arosio et al., 2023; Lioupa, 2023). The power of CoMMa stands in the speed of the delineation process (as demonstrated in our example), which allows for the creation of several tests in a short amount of time. Moreover, while in our case study we decided not to manually modify the semi-automated outputs for the statistical comparison, in an ordinary situation the user can intervene and edit the delineations where needed and use CoMMa purely for a rapid initial delineation.

In marine geomorphology and feature extraction a rapid and versatile delineation algorithm can benefit researchers for a consistent isolation of very large landform populations (e.g. pockmarks (Michel et al., 2017; Audsley et al., 2019), biogenic excavations (Schneider von Deimling et al., 2023) or seamounts (Gevorgian et al., 2023)). Additionally, CoMMa can be advantageous also in diachronic studies on landform evolution and multifaceted studies on landform structure. Dynamic landforms are common occurrences on the seabed, including current-induced (e.g. dunes and ribbons), fluid-flow (e.g. pockmarks and mud volcanoes) or biogenic features (e.g. excavations) (see Nanson et al., 2023). CoMMa is well-suited for repeated and reproducible landform measurements, leading to objective relative comparisons (the very same delineation method and thresholds can be used to different DEMs). Such application has been already tested with the unpublished delineation tool precursor of CoMMa on pockmarks by Gafeira and Long (2015a, 2015b).

Repeated delineations can be also useful to rapidly resolve different scientific questions on the same landform. An easy example is provided by the case study in this paper. Considering that small valleys or depressions within the bigger and composite Highway mounds may host ponded sediments and/or a different faunal assemblage, it may be useful to delineate both the total extent of the mounds and the valleys contained within them, for an in-depth morphological examination. Such different delineations can be easily achieved by using in turn both Boundary- and Element-based delineation. Alternatively, CoMMa can quickly be applied to separate nested size hierarchies of landforms (Minár et al., 2024), as for example landslide components, or nested pockmarks.

5.3. Limitations

CoMMa's flexibility comes at the cost of the rather heuristic procedure to find the best delineation method, input layers (that may require LTPs) and thresholds selection. These will depend on the

characteristics of the input DEM and the landforms to be mapped, and care should be taken to select the appropriate combination each time. Moreover, the heuristic approach requires some familiarity with the tool before the user can comfortably take advantage of all the features offered.

CoMMa neither does resolve the perennial problem of scale and semantic definition of a landform (Evans, 2012; Sofia, 2020; Minár et al., 2024). While multiple landform scales can be dealt with, as mentioned above in the case of nested landforms, by repeated runs of the algorithms with progressive parameter dimensions (one-size-fits-all solutions are not possible), landform semantic definitions are harder to convert to figures. CoMMa does not provide operational definitions for landform extraction (as described by Evans, 2012), and the user establishes what these are and how to implement them, if by decomposition (element-based) or by footprint (boundary based) (somewhat similarly to Sofia (2020)'s *de re* and de facto readings). Consistency in the adoption of these operational rules (or "semantic models") is essential to secure replicability and comparability (Wernette et al., 2018).

Finally, in terms of landform types, the Boundary-based delineation in CoMMa currently does not permit to map features that possess both positive and negative elementary facets. Therefore, landforms such as submarine calderas, landslides (considered in their entirety) or subaerial glacial cirques can be addressed only by using the Elements-based delineation.

6. Conclusions

The results shown in this study indicate that the CoMMa Toolbox is an efficient and fast alternative to manual mapping, providing a series of flexible solutions that can be applied to a suite of problems regarding confined morphology delineations. This set of semi-automated tools can also provide accurate, quantitative geomorphometric information critical to improve the understanding of the landform-seabed relationships, formation mechanisms and potential environmental drivers. Having quantified data extracted in a repeatable and replicable approach permits comparison of morphological variations in space or time.

Furthermore, problems encountered by marine geoscientists are also shared by terrestrial geomorphologists, and CoMMa tools may be utilised by planners and engineers especially in extensive or remote locations where the interpretation of DEMs is necessary, or in extra-terrestrial settings where the reliance on DEMs, when available, for geomorphological characterization has distinct advantages.

Supplementary data to this article can be found online at https://doi.org/10.1016/j.geomorph.2024.109227.

CRediT authorship contribution statement

Riccardo Arosio: Writing – review & editing, Writing – original draft, Visualization, Software, Methodology, Formal analysis, Data curation, Conceptualization. **Joana Gafeira:** Writing – review & editing, Methodology, Formal analysis, Conceptualization. **Laurence H. De Clippele:** Writing – review & editing, Conceptualization. **Andrew J. Wheeler:** Writing – review & editing, Project administration, Funding acquisition, Formal analysis. **Veerle A.I. Huvenne:** Writing – review & editing, Formal analysis. **Fabio Sacchetti:** Writing – review & editing, Funding acquisition, Formal analysis. **Luis A. Conti:** Writing – review & editing, Formal analysis. **Aaron Lim:** Writing – review & editing, Funding acquisition, Formal analysis.

Declaration of competing interest

The authors declare that they have no known competing financial interests or personal relationships that could have appeared to influence the work reported in this paper.

Data availability

Data will be made available on request.

Acknowledgments

We thank Ian Evans, Christopher Gomez, Yingkui Li and Devin Harrison for the helpful reviews of the manuscript. Riccardo Arosio received funding from the Irish Marine Institute's research grant PDOC 19/08/03. Joana Gafeira, Veerle Huvenne and Laurence De Clippele received funding from the European Union's Horizon 2020 project iAtlantic (Grant Agreement No. 818123). Veerle Huvenne also acknowledges funding from the European Research Council for the Starting Grant CODEMAP (Grant No. 258482) and from the Natural Environment Research Council (NERC) through the MAREMAP programme and the CLASS project (Grant No. NE/R015953/1). Joana Gafeira publishes with the permission of the Executive Director of the British Geological Survey (NERC). This work reflects the author's views, and the European Union is not responsible for any use that may be made of the information it contains.

References

Abdou, I.E., Pratt, W.K., 1979. Quantitative design and evaluation of enhancement/thresholding edge detectors. Proc. IEEE 67, 753–763. https://doi.org/10.1109/PROC.1979.11325.

Adam, C., Vidal, V., Bonneville, A., 2005. MiFil: a method to characterize seafloor swells with application to the south central Pacific: SEAFLOOR SWELLS. Geochem. Geophys. Geosyst. 6 (120), Q01003 https://doi.org/10.1029/2004GC000814.

Addamo, A.M., Vertino, A., Stolarski, J., García-Jiménez, R., Taviani, M., Machordom, A., 2016. Merging scleractinian genera: the overwhelming genetic similarity between solitary Desmophyllum and colonial Lophelia. BMC Evol. Biol. 16, 108. https://doi.org/10.1186/s12862-016-0654-8.

Andrews, B.D., Brothers, L.L., Barnhardt, W.A., 2010. Automated feature extraction and spatial organization of seafloor pockmarks, Belfast Bay, Maine, USA. Geomorphology 124, 55–64. https://doi.org/10.1016/j.geomorph.2010.08.009.

Arosio, R., Gafeira, J., 2023. CoMMa Toolbox v1.0. https://doi.org/10.5281/ZENODO.8434457.

Arosio, R., Mitchell, P., Hawes, J., Bolam, S., Benson, L., Sperry, J., 2021. Small Island Developing States (SIDS) and the sea: creating high resolution habitat maps to support effective marine management in St. Lucia. In: Presented at the EGU, Vienna. https://doi.org/10.5194/egusphere-egu21-102.

Arosio, R., Wheeler, A.J., Sacchetti, F., Guinan, J., Benetti, S., O'Keeffe, E., van Landeghem, K.J.J., Conti, L.A., Furey, T., Lim, A., 2023. The geomorphology of Ireland's continental shelf. J. Maps 19, 2283192. https://doi.org/10.1080/17445647.2023.2283192.

Audsley, A., Bradwell, T., Howe, J.A., Baxter, J.M., 2019. Distribution and classification of pockmarks on the seabed around western Scotland. J. Maps 15, 807–817. https://doi.org/10.1080/17445647.2019.1676320.

Bhadouria, V., 2023. Pratt's figure of Merit, MATLAB Central File Exchange. https://www.mathworks.com/matlabcentral/fileexchange/60473-pratt-s-figure-of-merit.

Cantwell, K., Wagner, A., Weinnig, A., Hoy, S., Dunn, C.J., Copeland, A., 2019. Windows to the Deep 2019: EX1903 Leg 2 (EX1903L2) Cruise Report, Southeast and Mid-Atlantic U.S Continental Margin, Port Canaveral, FL to Norfolk, VA (June 20–July, 12 2019), EX-19-03. NOAA, Silver Spring.

Cantwell, K., Sautter, L., Morrison, C., Sowers, D.C., Bowman, A., 2020. Cruise Report: EX-18-06, Windows to the Deep 2018 (ROV & Mapping), EX-18-06. NOAA, Silver Spring.

Cassol, W.N., Daniel, S., Guilbert, É., 2021. A segmentation approach to identify underwater dunes from digital bathymetric models. Geosciences 11, 361. https://doi.org/10.3390/geosciences11090361.

Conti, L.A., Lim, A., Wheeler, A.J., 2019. High resolution mapping of a cold water coral mound. Sci. Rep. 9, 1016. https://doi.org/10.1038/s41598-018-37725-x.

Cox, E.P., 1927. A method of assigning numerical and percentage values to the degree of roundness of sand grains. J. Paleontol. 1, 179–183.

De Clippele, L.H., Gafeira, J., Robert, K., Hennige, S., Lavaleye, M.S., Duineveld, G.C.A., Huvenne, V.A.I., Roberts, J.M., 2017. Using novel acoustic and visual mapping tools to predict the small-scale spatial distribution of live biogenic reef framework in cold-water coral habitats. Coral Reefs 36, 255–268. https://doi.org/10.1007/s00338-016-1519-8.

De Reu, J., Bourgeois, J., Bats, M., Zwertvaegher, A., Gelorini, V., De Smedt, P., Chu, W., Antrop, M., De Maeyer, P., Finke, P., Van Meirvenne, M., Verniers, J., Crombé, P., 2013. Application of the topographic position index to heterogeneous landscapes. Geomorphology 186, 39–49. https://doi.org/10.1016/j.geomorph.2012.12.015.

Di Stefano, M., Mayer, L., 2018. An automatic procedure for the quantitative characterization of submarine bedforms. Geosciences 8, 28. https://doi.org/10.3390/geosciences8010028.

Diesing, M., Thorsnes, T., 2018. Mapping of cold-water coral carbonate mounds based on geomorphometric features: an object-based approach. Geosciences 8, 34. https://doi.org/10.3390/geosciences8020034.
Eisank, C., Smith, M., Hillier, J., 2014. Assessment of multiresolution segmentation for delimiting drumlins in digital elevation models. Geomorphology 214, 452–464. https://doi.org/10.1016/j.geomorph.2014.02.028.
Evans, I.S., 2012. Geomorphometry and landform mapping: what is a landform? Geomorphology 137, 94–106. https://doi.org/10.1016/j.geomorph.2010.09.029.
Foroutan, M., Zimbelman, J.R., 2017. Semi-automatic mapping of linear-trending bedforms using 'Self-Organizing Maps' algorithm. Geomorphology 293, 156–166. https://doi.org/10.1016/j.geomorph.2017.05.016.
Gafeira, J., Long, D., 2015a. Geological Investigation of Pockmarks in the Braemar Pockmarks SCI (JNCC Report No. 571). JNCC, Peterborough.
Gafeira, J., Long, D., 2015b. Geological Investigation of Pockmarks in the Scanner Pockmark SCI Area (JNCC Report No. 570). JNCC, Peterborough.
Gafeira, J., Long, D., Diaz-Doce, D., 2012. Semi-automated characterisation of seabed pockmarks in the central North Sea. Near Surf. Geophys. 10, 301–312. https://doi.org/10.3997/1873-0604.2012018.
Gafeira, J., Dolan, M., Monteys, X., 2018. Geomorphometric characterization of pockmarks by using a GIS-based semi-automated toolbox. Geosciences 8, 154. https://doi.org/10.3390/geosciences8050154.
Gevorgian, J., Sandwell, D.T., Yu, Y., Kim, S.-S., Wessel, P., 2023. Global distribution and morphology of small seamounts. Earth Space Sci. 10, e2022EA002331 https://doi.org/10.1029/2022EA002331.
Gilbert, J.T., Macfarlane, W.W., Wheaton, J.M., 2016. The Valley Bottom Extraction Tool (V-BET): a GIS tool for delineating valley bottoms across entire drainage networks. Comput. Geosci. 97, 1–14. https://doi.org/10.1016/j.cageo.2016.07.014.
Goes, E.R., Brown, C.J., Araújo, T.C., 2019. Geomorphological classification of the benthic structures on a tropical continental shelf. Front. Mar. Sci. 6, 47. https://doi.org/10.3389/fmars.2019.00047.
Grosse, P., van Wyk de Vries, B., Euillades, P.A., Kervyn, M., Petrinovic, I.A., 2012. Systematic morphometric characterization of volcanic edifices using digital elevation models. Geomorphology 136, 114–131. https://doi.org/10.1016/j.geomorph.2011.06.001.
Hargrove, W.W., Hoffman, F.M., Hessburg, P.F., 2006. Mapcurves: a quantitative method for comparing categorical maps. J. Geogr. Syst. 8, 187–208. https://doi.org/10.1007/s10109-006-0025-x.
Harris, P., Macmillan-Lawler, M., Rupp, J., Baker, E., 2014. Geomorphology of the oceans. Mar. Geol. 352, 4–24.
Hillier, J.K., 2008. Seamount detection and isolation with a modified wavelet transform. Basin Res. 20, 555–573. https://doi.org/10.1111/j.1365-2117.2008.00382.x.
Hillier, J.K., Smith, M., 2008. Residual relief separation: digital elevation model enhancement for geomorphological mapping. Earth Surf. Process. Landf. 33, 2266–2276. https://doi.org/10.1002/esp.1659.
Hillier, J.K., Smith, M.J., 2012. Testing 3D landform quantification methods with synthetic drumlins in a real digital elevation model. Geomorphology 153–154, 61–73. https://doi.org/10.1016/j.geomorph.2012.02.009.
Hillier, J.K., Watts, A.B., 2004. "'Plate-like"' subsidence of the East Pacific Rise–South Pacific superswell system. J. Geophys. Res. 109 https://doi.org/10.1029/2004JB003041.
Hillier, J.K., Smith, M.J., Armugam, R., Barr, I., Boston, C.M., Clark, C.D., Ely, J., Frankl, A., Greenwood, S.L., Gosselin, L., Hättestrand, C., Hogan, K., Hughes, A.L.C., Livingstone, S.J., Lovell, H., McHenry, M., Munoz, Y., Pellicer, X.M., Pellitero, R., Robb, C., Roberson, S., Ruther, D., Spagnolo, M., Standell, M., Stokes, C.R., Storrar, R., Tate, N.J., Wooldridge, K., 2015a. Manual mapping of drumlins in synthetic landscapes to assess operator effectiveness. J. Maps 11, 719–729. https://doi.org/10.1080/17445647.2014.957251.
Hillier, J.K., Sofia, G., Conway, S.J., 2015b. Perspective – synthetic DEMs: a vital underpinning for the quantitative future of landform analysis? Earth Surf. Dynam. 3, 587–598. https://doi.org/10.5194/esurf-3-587-2015.
Huang, Z., Nanson, R., McNeil, M., Wenderlich, M., Gafeira, J., Post, A., Nichol, S., 2023. Rule-based semi-automated tools for mapping seabed morphology from bathymetry data. Front. Mar. Sci. 10, 1236788 https://doi.org/10.3389/fmars.2023.1236788.
Huvenne, V.A.I., 2011. Benthic habitats and the impact of human activities in Rockall Trough, on Rockall Bank and in Hatton Basin. In: RRS James Cook Cruise 60 (National Oceanography Centre Cruise Report No. 4). National Oceanography Centre, Southampton.
Huvenne, V.A.I., De Mol, B., Henriet, J.-P., 2003. A 3D seismic study of the morphology and spatial distribution of buried coral banks in the Porcupine Basin, SW of Ireland. Mar. Geol. 198, 5–25. https://doi.org/10.1016/S0025-3227(03)00092-6.
Huvenne, V.A.I., Masson, D.G., Wheeler, A.J., 2009. Sediment dynamics of a sandy contourite: the sedimentary context of the Darwin cold-water coral mounds, Northern Rockall Trough. Int. J. Earth Sci. (Geol. Rundsch.) 98, 865–884. https://doi.org/10.1007/s00531-008-0312-5.
Jarna, A., Baeten, N.J., Elvenes, S., Bellec, V.K., Thorsnes, T., Diesing, M., 2019. Semi-automatic versus manual mapping of cold-water coral carbonate mounds located offshore Norway. IJGI 8, 40. https://doi.org/10.3390/ijgi8010040.
Jasiewicz, J., Stepinski, T.F., 2013. Geomorphons — a pattern recognition approach to classification and mapping of landforms. Geomorphology 182, 147–156. https://doi.org/10.1016/j.geomorph.2012.11.005.
Jorge, M.G., Brennand, T.A., 2017. Semi-automated extraction of longitudinal subglacial bedforms from digital terrain models – two new methods. Geomorphology 288, 148–163. https://doi.org/10.1016/j.geomorph.2017.04.001.
Kim, S.-S., Wessel, P., 2008. Directional median filtering for regional-residual separation of bathymetry: TECHNICAL BRIEF. Geochem. Geophys. Geosyst. 9 (3), Q03005 https://doi.org/10.1029/2007GC001850.
Lebrec, U., Riera, R., Paumard, V., O'Leary, M.J., Lang, S.C., 2022. Automatic mapping and characterisation of linear depositional bedforms: theory and application using bathymetry from the North West Shelf of Australia. Remote Sens. 14, 280. https://doi.org/10.3390/rs14020280.
Lecours, V., 2017. TASSE (Terrain Attribute Selection for Spatial Ecology) Toolbox v. 1.1. https://doi.org/10.13140/RG.2.2.15014.52800.
Li, Y., Evans, I.S., Spagnolo, M., Pellitero, R., Barr, I.D., Ely, J.C., 2024. ACME2: an extended toolbox for automated cirque metrics extraction. Geomorphology 445, 108982. https://doi.org/10.1016/j.geomorph.2023.108982.
Lindsay, J.B., Cockburn, J.M.H., Russell, H.A.J., 2015. An integral image approach to performing multi-scale topographic position analysis. Geomorphology 245, 51–61. https://doi.org/10.1016/j.geomorph.2015.05.025.
Linklater, M., Ingleton, T.C., Kinsela, M.A., Morris, B.D., Allen, K.M., Sutherland, M.D., Hanslow, D.J., 2019. Techniques for classifying seabed morphology and composition on a subtropical-temperate continental shelf. Geosciences 9, 141. https://doi.org/10.3390/geosciences9030141.
Lioupa, V., 2023. Comparing Manual and Semi-Automated Methods for Deducing Geomorphometric Characteristics of Miniature Biogenic Reefs in a Shallow Land-locked Gulf of the Aegean Sea.
Lundblad, E.R., Wright, D.J., Miller, J., Larkin, E.M., Rinehart, R., Naar, D.F., Donahue, B.T., Anderson, S.M., Battista, T., 2006. A benthic terrain classification scheme for American Samoa. Mar. Geod. 29, 89–111. https://doi.org/10.1080/01490410600738021.
Michel, G., Dupré, S., Baltzer, A., Ehrhold, A., Imbert, P., Pitel, M., Loubrieu, B., Scalabrin, C., Lazure, P., Marié, L., Geldof, J.-B., Deville, É., 2017. Pockmarks on the South Aquitaine Margin continental slope: the seabed expression of past fluid circulation and former bottom currents. Compt. Rendus Geosci. 349, 391–401. https://doi.org/10.1016/j.crte.2017.10.003.
Minár, J., Drăguţ, L., Evans, I.S., Feciskanin, R., Gallay, M., Jenčo, M., Popov, A., 2024. Physical geomorphometry for elementary land surface segmentation and digital geomorphological mapping. Earth Sci. Rev. 248, 104631 https://doi.org/10.1016/j.earscirev.2023.104631.
Nanson, R., Arosio, R., Gafeira, J., McNeil, M., Dove, D., Bjarnadóttir, L., Dolan, M., Guinan, J., Post, A., Webb, J., Nichol, S., 2023. A Two-part Seabed Geomorphology Classification Scheme; Part 2: Geomorphology Classification Framework and Glossary (Version 1.0). Zenodo. https://doi.org/10.5281/zenodo.7804019.
Newman, D.R., Lindsay, J.B., Cockburn, J.M.H., 2018. Evaluating metrics of local topographic position for multiscale geomorphometric analysis. Geomorphology 312, 40–50. https://doi.org/10.1016/j.geomorph.2018.04.003.
Nielsen, S.E., Herrero, S., Boyce, M.S., Mace, R.D., Benn, B., Gibeau, M.L., Jevons, S., 2004. Modelling the spatial distribution of human-caused grizzly bear mortalities in the Central Rockies ecosystem of Canada. Biol. Conserv. 120, 101–113. https://doi.org/10.1016/j.biocon.2004.02.020.
Palafox, L.F., Hamilton, C.W., Scheidt, S.P., Alvarez, A.M., 2017. Automated detection of geological landforms on Mars using Convolutional Neural Networks. Comput. Geosci. 101, 48–56. https://doi.org/10.1016/j.cageo.2016.12.015.
Panagiotakis, C., Kokinou, E., 2017. Unsupervised detection of topographic highs with arbitrary basal shapes based on volume evolution of isocontours. Comput. Geosci. 102, 22–33. https://doi.org/10.1016/j.cageo.2017.02.004.
Rockafellar, R.T., Wets, R.J.-B., 2004. Variational analysis. In: Grundlehren der mathematischen Wissenschaften, Corr. 2nd print. ed. Springer, Berlin.
Roux, C., Alber, A., Bertrand, M., Vaudor, L., Piégay, H., 2015. "FluvialCorridor": a new ArcGIS toolbox package for multiscale riverscape exploration. Geomorphology 242, 29–37. https://doi.org/10.1016/j.geomorph.2014.04.018.
Saha, K., Van Landeghem, K.J.J., 2021. Evaluating an automated object-oriented method to delineate drumlins from both terrestrial and submarine digital elevation models. In: ISPRS Ann. Photogramm. Remote Sens. Spatial Inf. Sci. V-3–2021, pp. 29–35. https://doi.org/10.5194/isprs-annals-V-3-2021-29-2021.
Saha, K., Wells, N.A., Munro-Stasiuk, M., 2011. An object-oriented approach to automated landform mapping: a case study of drumlins. Comput. Geosci. 37, 1324–1336. https://doi.org/10.1016/j.cageo.2011.04.001.
Sappington, J.M., Longshore, K.M., Thompson, D.B., 2007. Quantifying landscape ruggedness for animal habitat analysis: a case study using bighorn sheep in the Mojave Desert. J. Wildl. Manag. 71, 1419–1426. https://doi.org/10.2193/2005-723.
Sărășan, A., Józsa, E., Ardelean, A.C., Drăguţ, L., 2019. Sensitivity of geomorphons to mapping specific landforms from a digital elevation model: a case study of drumlins. Area 51, 257–267. https://doi.org/10.1111/area.12451.
Scheiber, T., Fredin, O., Viola, G., Jarna, A., Gasser, D., Łapińska-Viola, R., 2015. Manual extraction of bedrock lineaments from high-resolution LiDAR data: methodological bias and human perception. GFF 137, 362–372. https://doi.org/10.1080/11035897.2015.1085434.
Schneider von Deimling, J., Hoffmann, J., Geersen, J., Koschinski, S., Lohrberg, A., Gilles, A., Belkin, I., Böttner, C., Papenmeier, S., Krastel, S., 2023. Millions of seafloor pits, not pockmarks, induced by vertebrates in the North Sea. Commun. Earth Environ. 4, 1–10. https://doi.org/10.1038/s43247-023-01102-y.
Smith, M.J., Wise, S.M., 2007. Problems of bias in mapping linear landforms from satellite imagery. Int. J. Appl. Earth Obs. Geoinf. 9, 65–78. https://doi.org/10.1016/j.jag.2006.07.002.
Smith, M.J., Rose, J., Gousie, M.B., 2009. The Cookie Cutter: a method for obtaining a quantitative 3D description of glacial bedforms. Geomorphology 108, 209–218. https://doi.org/10.1016/j.geomorph.2009.01.006.
Sofia, G., 2020. Combining geomorphometry, feature extraction techniques and Earth-surface processes research: the way forward. Geomorphology 355, 107055. https://doi.org/10.1016/j.geomorph.2020.107055.

Summers, G., Lim, A., Wheeler, A.J., 2021. A scalable, supervised classification of seabed sediment waves using an object-based image analysis approach. Remote Sens. 13, 2317. https://doi.org/10.3390/rs13122317.

Walbridge, S., Slocum, N., Pobuda, M., Wright, D.J., 2018. Unified geomorphological analysis workflows with benthic terrain modeler. Geosciences 8, 94.

Weiss, A.D., 2001. Topographic positions and landforms analysis. In: Presented at the ESRI International User Conference, Indus Corporation. Aweiss@induscorp.com, San Diego, California.

Wernette, P., Thompson, S., Eyler, R., Taylor, H., Taube, C., Medlin, A., Decuir, C., Houser, C., 2018. Defining dunes: evaluating how dune feature definitions affect dune interpretations from remote sensing. J. Coast. Res. 34, 1460. https://doi.org/10.2112/JCOASTRES-D-17-00082.1.

Wessel, P., 1998. An empirical method for optimal robust regional-residual separation of geophysical data. Math. Geol. 30, 18.

Wessel, P., 2016. Regional–residual separation of bathymetry and revised estimates of Hawaii plume flux. Geophys. J. Int. 204, 932–947. https://doi.org/10.1093/gji/ggv472.

Wheeler, A.J., Kozachenko, M., Masson, D.G., Huvenne, V.A.I., 2008. Influence of benthic sediment transport on cold-water coral bank morphology and growth: the example of the Darwin Mounds, north-east Atlantic. Sedimentology 55, 1875–1887. https://doi.org/10.1111/j.1365-3091.2008.00970.x.

Yu, P., Eyles, N., Sookhan, S., 2015. Automated drumlin shape and volume estimation using high resolution LiDAR imagery (Curvature Based Relief Separation): a test from the Wadena Drumlin Field, Minnesota. Geomorphology 246, 589–601. https://doi.org/10.1016/j.geomorph.2015.07.020.